

Long-term monitoring in IC4665: Fast rotation and weak variability in very low mass objects

Alexander Scholz^{1*}, Jochen Eisloffel^{2†} and Reinhard Mundt³

¹*SUPA, School of Physics & Astronomy, University of St. Andrews, North Haugh, St. Andrews, Fife KY16 9SS, United Kingdom*

²*Thüringer Landessternwarte Tautenburg, Sternwarte 5, D-07778 Tautenburg, Germany*

³*Max-Planck-Institut für Astronomie, Königstuhl 17, D-69117 Heidelberg, Germany*

Accepted. Received.

ABSTRACT

We present the combined results of three photometric monitoring campaigns targeting very low mass (VLM) stars and brown dwarfs in the young open cluster IC4665 (age ~ 40 Myr). Each of our observing runs covers timescales of ~ 5 days in the seasons 1999, 2001, 2002, respectively. In all three runs, we observe ~ 100 cluster members, allowing us for the first time to put limits on the evolution of spots and magnetic activity in fully convective objects on timescales of a few years. For 20 objects covering masses from 0.05 to $0.5 M_{\odot}$ we detect a periodic flux modulation, indicating the presence of magnetic spots co-rotating with the objects. The detection rate of photometric periods ($\sim 20\%$) is significantly lower than in solar-mass stars at the same age, which points to a mass dependence in the spot properties. With two exceptions, none of the objects exhibit variability and thus spot activity in more than one season. This is contrary to what is seen in solar-mass stars and indicates that spot configurations capable of producing photometric modulations occur relatively rarely and are transient in VLM objects. The rotation periods derived in this paper range from 3 to 30 h, arguing for a lack of slow rotators among VLM objects. The periods fit into a rotational evolution scenario with pre-main sequence contraction and moderate (40-50%) angular momentum losses due to wind braking. By combining our findings with literature results, we identify two regimes of rotational and magnetic properties, called C- and I-sequence. Main properties on the C-sequence are fast rotation, weak wind braking, $H\alpha$ emission, and saturated activity levels, while the I-sequence is characterised by slow rotation, strong wind braking, no $H\alpha$ emission, and linear activity-rotation relationship. Rotation rate and stellar mass are the primary parameters that determine in which regime an object is found. We outline a general scheme to understand rotational evolution for low-mass objects in the context of these two regimes and discuss the potential as well as the problems of this scheme.

Key words: stars: low-mass, brown dwarfs, stars: rotation, stars: evolution, stars: activity

1 INTRODUCTION

Rotation and magnetic activity are key parameters of stellar evolution. While these parameters have been well-explored for solar-mass stars over the past decades, our knowledge is still sparse in the very low mass (VLM) regime. The interest in rotation and activity in VLM stars and brown dwarfs is fueled by the hypothesis that these properties depend on a fundamental level on the interior structure. Specifically, to operate the type of dynamo that generates the solar-

type cyclical magnetic field, the presence of a shear layer between convective envelope and radiative core is thought to be of prime importance (e.g. Spiegel & Weiss 1980; Spruit & van Ballegoijen 1982, and references therein). Objects with masses $\lesssim 0.3 M_{\odot}$, however, are fully convective throughout their evolution (Chabrier & Baraffe 1997). Thus, if the aforementioned assumptions are correct, they would not be able to generate magnetic fields in the same way as solar-type stars. Changes in magnetic properties and, consequently, rotational evolution are therefore expected at the fully-convective boundary (see Delfosse et al. 1998).

Rotation and activity are interdependent in a twofold sense: On one side, rotation plays an important role in driv-

* E-mail: as110@st-andrews.ac.uk

† E-mail: jochen@tls-tautenburg.de

ing the dynamo and essentially powers magnetic activity. On the other side, stellar winds driven by magnetic fields are the predominant agent of the spindown on the main-sequence and thus determine the long-term rotational evolution of stars. For solar-mass stars, the close connection between rotation and activity manifests itself in the rotation/activity relation, which is linear for slow rotators and flattens at high rotation rates, as well as in the Skumanich law (Skumanich 1972), which establishes that rotation rates and activity indicators both decline with the square root of age on the main-sequence.

Over the past decade, it has been shown convincingly that, with the exception of a few very young objects, VLM stars and brown dwarfs are fast rotators with periods generally shorter than 2 d (e.g. Bailer-Jones & Mundt 2001; Scholz & Eislöffel 2004b; Herbst et al. 2007; Reiners & Basri 2008; Rodríguez-Ledesma et al. 2009). The periods found in the Monitor project confirm this finding (see in particular Irwin et al. 2008b). Rotational braking due to stellar winds is clearly less efficient in this mass regime. On the other hand, a number of ultracool objects are now known to harbour strong, large-scale magnetic fields, as evidenced by Zeeman Doppler imaging (Donati et al. 2008; Morin et al. 2008b), direct field measurements (Reiners & Basri 2007), and radio observations (e.g. Berger 2006; Hallinan et al. 2006). A full theory that accounts for all these findings is still missing.

Investigating rotation and activity in the VLM regime therefore has the potential to probe fundamental physical questions: To what extent does interior structure affect the observable properties of stars? How does magnetic field generation change as a function of object mass? Can we successfully predict rotation rates for a given age and mass? The latter problem leads to the intriguing possibility to use rotation periods – a quantity that can be measured with high accuracy – to determine stellar ages and masses (gyrochronology, see Barnes 2007).

The goal of this paper is to provide new observational constraints on rotation and activity in the very low mass regime. We will probe a specific subset of magnetic phenomena, namely the properties of magnetically induced spots in the photosphere. We present results from three photometric monitoring campaigns in the young open cluster IC4665, including 20 new rotation periods for VLM stars and brown dwarfs (Sect. 2-4). Through repeated monitoring, we are able to probe the characteristics and the long-term evolution of magnetic spots in this critical mass regime (Sect. 5). Finally, we will use our periods in combination with literature data to probe rotational braking and magnetic properties in low-mass objects (Sect. 6 and 7).

2 PHOTOMETRIC MONITORING AND DATA REDUCTION

2.1 Observations

The target field for this variability study covers parts of the central region of the open cluster IC4665. The field is centred at $17^h 45^m 15.0^s \delta + 05^\circ 21' 17''.0$ (J2000.0) and is covered by our photometric survey (Eislöffel et al., in prep., see Sect. 3). This region was observed in three I-band monitoring campaigns covering a time span of four years in total, using the

Table 1. Observing log for the three observing runs, runs A and C were carried out with the ESO/MPG 2.2-m WFI, run B with the TLS Schmidt camera. Columns 3-6 contain number of exposures, integration time per exposure, sky conditions, median seeing.

run	date	no.	exp. time	weather	seeing
A	28/05/1999	1	600 s	photometric	1''2
	05/06/1999	44	500 s	some cirrus	0''7
	06/06/1999	43	500 s	photometric	0''9
	08/06/1999	3	500 s	partly cloudy	1''2
	09/06/1999	5	500 s	photometric	1''2
B	19/05/2001	13	600 s	partly cloudy	3''4
	20/05/2001	24	600 s	some cirrus	2''7
	21/05/2001	23	600 s	partly cloudy	2''9
	22/05/2001	23	600 s	photometric	2''6
	23/05/2001	22	600 s	photometric	2''6
C	29/05/2002	15	500 s	photometric	1''6
	07/06/2002	14	500 s	partly cloudy	1''2
	08/06/2002	14	500 s	photometric	1''3
	09/06/2002	10	500 s	some cirrus	1''5
	12/06/2002	17	500 s	some cirrus	1''6
	13/06/2002	17	500 s	some cirrus	1''3

ESO/MPG 2.2-m Wide Field Imager at La Silla and the 2-m Schmidt telescope at the Thüringer Landessternwarte (TLS). Both instruments have a comparable field of view of ~ 0.32 sqdeg.

Details for the three observing runs are given in Table 1. In the first WFI run in May/June 1999, we took 96 long exposure images of this field, including complete coverage of two consecutive nights. The second WFI run was carried out in service mode, resulting in dense coverage of typically 2-3 h per night for six nights distributed over two weeks. This campaign provided 87 time series images of our field in IC4665. The TLS observing run covers five consecutive nights with typically 4 h of continuous observations per night, in total 105 exposures. The TLS time series suffered from bright sky background and sub-optimal seeing, and thus the photometric accuracy was significantly lower than in the WFI runs. The typical integration time for individual exposures was 500 sec in all three runs.

2.2 Image reduction

All images were reduced in a similar fashion, following the recipes outlined in Scholz & Eislöffel (2004a, 2005). The reduction includes bias subtraction and flatfield correction using either twilight flats (WFI) or domeflats (TLS). Additionally, the I-band images have to be corrected for multiplicatively large-scale illumination gradients, a consequence of imperfect flatfielding, and additive, small-scale fringe structures. Both effects can be corrected using a 'superflat' constructed from images of dark sky regions. By median-filtering the superflat, large-scale structures (illumination) can be separated from the small-scale fringes. As a result, we obtain an image of the average illumination and the average fringe pattern. Since fringes are variable as a function of airmass, temperature, and weather conditions, an appropriate scaling is required for each time series image. We used the automated scaling procedure outlined in Scholz & Eislöffel (2005), and manually refined the resulting scaling factors if

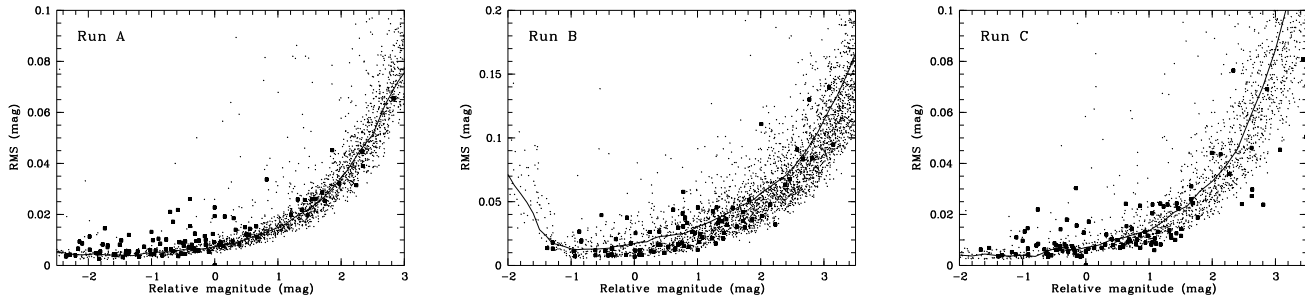


Figure 1. RMS vs. relative magnitude for all three runs: solid lines show the binned median rms, large symbols the VLM candidate members. Note the different scale on the y-axis of the middle panel. For run B, we only plot 4000 of 10000 field objects, for clarity. Due to the differences in the I-band filters used in the various campaigns, the relative magnitudes are not easily transformed to calibrated I-band photometry. The approximate I-band mags for the zeropoint on the relative scale are 17.2, 16.2, and 16.5 mag for runs A-C, respectively, with an uncertainty of ± 0.3 mag. These numbers are derived by comparing the relative magnitudes with the absolute photometry derived in our survey (Sect. 3).

necessary. We estimate the residuals after fringe correction to be not larger than 1% of the sky background.

2.3 Instrumental magnitudes

We derived instrumental magnitudes for all objects in the time series field by fitting their point spread function (PSF) using the *daophot* package within IRAF (Stetson 1987). For the WFI runs, all photometry steps were done on each chip of the mosaic separately to account for the variable properties of the CCDs, e.g. the nonlinearity of the chip response.

Model PSFs were calculated using typically 40 isolated stars. Then, this model was fit to each object in the field. The reliability of the resulting photometry was checked by subtracting all PSF fits from the original image. As result we obtained essentially empty frames, in which only saturated objects, bright galaxies, and some close undetected binary companions remained.

2.4 Relative calibration

The lightcurves of all objects were calibrated relatively with an average lightcurve from a set of non-variable reference stars in the observed field. The selection of reference stars was performed in a similar fashion for all three campaigns, using the procedure described in Scholz & Eislöffel (2004a). In short, the routine compares each potential reference star with the average of all other potential reference stars. For the WFI runs, this procedure was again carried out for each chip of the mosaic separately. Typically, the final sample of reference stars comprises of ~ 100 objects per chip. From these objects, the final reference lightcurve was determined. By subtracting this reference lightcurve from all time series from the respective observing run, we obtained relatively calibrated magnitudes for all objects.

In Fig. 1 a-c we plot the lightcurve RMS vs. relative magnitude for all three runs. Overplotted is the median rms per magnitude bin as solid line after excluding outliers – this function gives the typical photometric error at a given relative magnitude. For bright, unsaturated stars with I-band magnitudes of 15-16, we obtain average uncertainties of 5-8 mmag in runs A and C and 10-20 mmag in run B. Over-

plotted in large symbols in Fig. 1 are the datapoints for the sample of cluster member candidates, described in Sect. 3.

3 THE SAMPLE OF PROBABLE CLUSTER MEMBERS

The targets for our variability analysis are 113 sources classified as probable cluster members in our deep photometric survey in IC4665. The detailed outcomes of this survey will be published in a forthcoming paper (Eislöffel et al., in prep.). In short: We surveyed ~ 0.4 sqdeg of the central cluster in the R- and I-band using the ESO/MPG WFI at the 2.2-m telescope at La Silla – these images have been obtained in the same observing run that provided the first time series (run A, see Sect. 2.1). The R- and I-band data is calibrated by comparing with photometry of Landolt standard fields observed in the same nights (Landolt 1992). A deep (I,R-I) colour magnitude diagram yielded a sample of 118 objects whose optical colours are consistent with an empirically determined isochrone for the cluster IC4665 (see Fig. 2). We complemented the survey with near-infrared photometry, either from 2MASS or from our own J-band data¹. From the primary sample, 112 objects show near-infrared colours in agreement with the model isochrone for an age of 40 Myr from Baraffe et al. (1998).

Furthermore, we surveyed a larger area of the cluster with the 2-m Schmidt telescope at the Thüringer Landessternwarte Tautenburg in a run in May 1999. The I-band photometry from this campaign combined with 2MASS near-infrared data yielded an (I,I-J) colour-magnitude diagram. Applying a colour selection, we obtained an additional sample of 57 probable cluster members. Only one of these sources is located in the monitoring field and shows a significant period in run A of the variability study (object #119, see below). We include this object in the discussion. Thus, the sample for the time series analysis comprises 113 objects, with calibrated photometry in optical and near-infrared bands.

¹ Observations carried out with the near-infrared camera Ω' at the 3.5-m telescope on Calar Alto/Spain, Deutsch-Spanisch Astronomisches Zentrum

Table 2. Basic data (coordinates, photometry, masses) for the cluster member candidates with periodic lightcurve in at least one of the monitoring campaigns. Full survey results to be published in Eislöffel et al. (in prep.). "2M" indices designate photometry from the 2MASS database. Mass estimates derived by comparing the near-infrared photometry with evolutionary tracks by Baraffe et al. (1998).

ID	α (J2000.0)	δ	R (mag)	I (mag)	J (mag)	J _{2M} (mag)	H _{2M} (mag)	K _{2M} (mag)	Mass (M_{\odot})
7	17 43 59.64	5 17 37.8	19.43	17.54	15.90	15.82	15.32	14.95	0.14
28	17 44 30.17	5 18 49.2	17.86	16.40	14.89	14.91	14.33	13.93	0.27
31	17 44 31.46	5 34 09.3	20.70	18.51	16.68				0.09
36	17 44 42.84	5 19 24.8	20.29	18.13	15.94	16.05	15.28	15.25	0.12
37	17 44 43.23	5 09 20.6	19.79	17.64	15.67	15.78	15.06	15.00	0.14
39	17 44 44.08	5 21 09.7	17.59	15.74	13.90	13.93	13.31	13.00	0.51
40	17 44 46.45	5 32 01.9	20.04	17.83	16.16	15.77	15.28	14.89	0.14
49	17 44 54.68	5 23 52.4	17.71	16.07	14.24	14.49	13.78	13.56	0.37
55	17 45 05.57	5 11 11.0	18.11	16.34	14.67	14.67	14.01	13.78	0.32
57	17 45 06.69	5 30 38.4	18.69	16.79	15.28	15.07	14.41	14.01	0.25
59	17 45 10.95	5 33 28.5	19.14	17.14	15.53	15.43	14.67	14.49	0.19
63	17 45 13.53	5 18 39.2	17.90	16.08	14.33	14.32	13.73	13.36	0.41
73	17 45 21.39	5 34 37.8	19.39	17.32	15.73	15.48	14.80	14.59	0.18
75	17 45 26.00	5 29 40.5	20.98	18.48	16.56	16.21	15.63	15.24	0.11
76	17 45 27.20	5 33 57.8	23.00	20.32	18.00				0.05
88	17 45 37.44	5 23 40.5	19.44	17.63	15.88	15.95	15.27	15.00	0.13
100	17 45 49.89	5 09 40.2	18.23	16.32	14.61	14.66	13.97	13.64	0.34
110	17 45 59.35	5 29 31.6	20.57	18.24	16.32	16.01	15.44	15.12	0.12
118	17 46 06.29	5 36 39.3	20.87	18.50					0.09
119	17 45 37.10	5 23 08.1	15.79			14.28	13.63	13.34	0.42

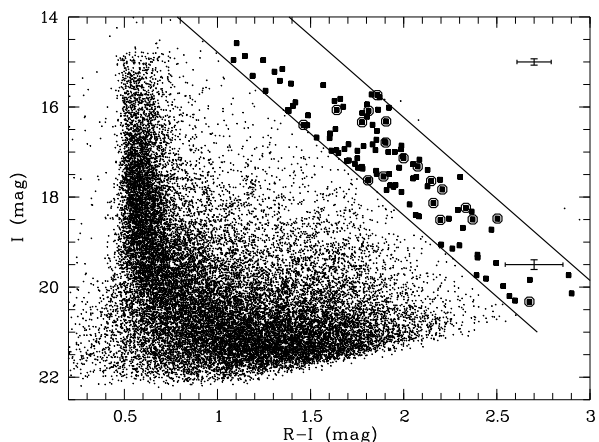


Figure 2. I,R-I colour magnitude diagram for our time series field in IC4665: The two solid lines illustrate the colour criterium applied to select the primary sample. All probable cluster members according to their colours are shown as large dots; objects with periodic lightcurve are marked with squares. Errorbars indicate typical photometric uncertainties. For clarity, only ~ 10000 out of ~ 30000 total datapoints are shown. Photometry obtained during run A (see Table 1). Missing from that figure is object no. 119, which was identified in a different campaign (see text).

The photometrically selected cluster member candidates may be contaminated by red field objects. The contamination rate was estimated based on optical colour-magnitude diagrams simulated using the Galaxy model presented by Robin & Creze (1986) and Robin et al. (2003). We derive a contamination rate of $\sim 30\%$ for the total candidate sample, most of the contaminating objects are expected to be M dwarfs in the fore- or background of the cluster. From the space density for M dwarfs given by Reid & Gizis (1997)

and our survey area follows a contamination rate of about 30%, consistent with the Galaxy model.

In Fig. 2 we show the (I,R-I) colour magnitude diagram, probably cluster members are marked. In our three monitoring campaigns, we found 20 objects with significant periodicity in the lightcurve (see Sect. 4); these objects are marked with open circles. As can be seen in this plot, the majority of the periodic objects forms a tight sequence with less scatter than the total sample, as expected for objects on the cluster isochrone. This may be seen as evidence for lower contamination among the objects with period, although for a definite decision spectroscopy is required.

In Table 2 we provide the basic data for all objects in our survey with period detection in at least one of the monitoring campaigns. We estimate masses for these objects by comparing their near-infrared magnitudes with the cluster isochrone from Baraffe et al. (1998), assuming an age of 40 Myr, a distance of 350 pc, and an extinction of $E_{B-V} = 0.18$ (Mermilliod 1981a,b). According to this estimate, the objects span a mass range from 0.05 to $0.5M_{\odot}$ and thus include a few brown dwarf candidates. Due to uncertainties in the theoretical evolutionary tracks and differences between the standard bands and the filters used in the survey, resulting in calibration offsets, the mass estimates may be inaccurate by as much as 100%, particularly at very low masses. Since both effects are systematic, the masses for our objects are comparable on a relative scale.

4 TIME SERIES ANALYSIS

The main focus of the time series analysis was the search for periodic variabilities. The period search is described in detail in Sect. 4.1. In addition, we looked for conspicuous signs for clear non-periodic variability in the lightcurves: All candi-

date lightcurves were inspected visually to register obvious signs of rapid variability. In particular, we searched for signs of flares, i.e. for brightness eruptions with gradual decline lasting several hours. No such events with > 0.1 mag amplitude were found, indicating that flare events are rare in VLM objects. Based on our time coverage, we estimate an I-band flare rate of $< 3.2 \cdot 10^{-4} h^{-1}$, in agreement with the result obtained in a previous paper ($2.3 \cdot 10^{-4} h^{-1}$, Scholz & Eislöffel 2005).

In the RMS vs. magnitude plots in Fig. 1, we mark the cluster members with larger symbols, to allow an assessment of the generic variability. As can be seen in these plots, VLM objects in IC4665 show only low-level photometric variations, with amplitudes < 0.05 mag. Most of the objects that are observed to have an RMS significantly larger than the field average are later identified as objects with periodic variability. This is in contrast to the findings for field L dwarfs with similar masses, where variable objects are rarely found to exhibit a photometric period (e.g., Bailer-Jones & Mundt 2001; Gelino et al. 2002).

4.1 Period search for runs A and C

We used the Scargle periodogram (Scargle 1982) to identify candidate periods in the lightcurves from runs A and C. For the initial detection, we relied on a preliminary significance estimate based on the equation given by Horne & Baliunas (1986). All candidate periods are then verified in a number of independent tests. In particular, periodograms and lightcurves of possible periodic objects were compared with those of nearby stars and excluded if the neighbours show a similar periodicity. In addition, we CLEANed the periodograms for all periodic objects from sampling artefacts and aliases using the procedure given by Roberts et al. (1987) and checked if the peak found in the Scargle periodogram is still present. Only periods which pass all tests are accepted. The period search procedure is described in detail in Scholz & Eislöffel (2004a) and has been thoroughly tested in previous campaigns (Scholz & Eislöffel 2004b, 2005).

From the 113 VLM members in IC4665, 16 show significant periodic variability in run A and 6 in run C. Only two of these objects exhibit a photometric period in both campaigns. Final false alarm probabilities for the periodicities are estimated using the 'bootstrap' approach: For each candidate, a set of 10000 random lightcurves was generated by shuffling the photometry datapoints, while retaining the time sampling. The highest peak in the Scargle periodogram was determined for all these test lightcurves, and compared with the peak height found for the periodicity in the actual lightcurve. A $FAP < 0.01\%$ indicates that none of the 10000 random time series resulted in a Scargle peak higher than the one in the observed lightcurves. All our periods turn out to be highly significant according to this test. Table 3 lists the derived periods and further results from the time series analysis. The period errors ΔP in the table are determined following Horne & Baliunas (1986); for comparison we also derived ΔP from the FWHM of the peak in the Scargle periodogram which typically gives 1-3% uncertainty. The amplitudes in the table correspond to the peak-to-peak amplitude of a sinefit to the lightcurve, not the lightcurve itself, to avoid being affected by the noise in the photometry.

An assessment of the completeness of the period search

Table 3. Results of the period search: objects with significant periodic variability in runs A and B. (id: identification number from Table 2); P: period; ΔP : period error; A: amplitude (see text); FAP: false alarm probability (see text); N: number of datapoints used in the time series analysis

ID	P (h)	ΔP (h)	A (mag)	FAP (%)	N
Run A:					
7	3.64	0.08	0.009	0.03	91
31	2.99	0.02	0.019	< 0.01	91
36	5.45	0.01	0.045	< 0.01	93
37	6.72	0.02	0.027	< 0.01	89
40	16.5	0.08	0.047	< 0.01	94
49	5.36	0.08	0.006	< 0.01	90
55	7.69	0.06	0.007	< 0.01	92
57	10.3	0.06	0.022	< 0.01	95
59	14.0	0.04	0.045	< 0.01	93
63	9.56	0.23	0.015	< 0.01	88
76	4.26	0.02	0.052	0.05	92
88	3.14	0.02	0.012	0.07	93
100	5.99	0.02	0.010	< 0.01	93
110	9.16	0.04	0.033	< 0.01	93
118	4.49	0.06	0.122	< 0.01	92
119	5.81	0.11	0.005	< 0.01	84
Run C:					
28	4.56	0.02	0.011	0.03	86
39	9.20	0.03	0.020	< 0.01	73
57	16.3	0.12	0.022	< 0.01	87
59	14.4	0.04	0.072	< 0.01	86
73	27.0	0.35	0.028	< 0.01	87
75	4.84	0.02	0.033	< 0.01	87

can be made based on the time sampling in our observing campaigns. The upper frequency limit for the period search, thus the lower period limit, is frequently given as $\nu_{\max} = 1/2\delta$, where δ is the minimum separation between two datapoints (e.g. Roberts et al. 1987). For our WFI time campaigns, this gives a minimum period of $P_{\min} = 0.4 h$. Since we did not find any period with $P < 3 h$, we are complete at short periods. With regular sampling, the longest period than can reliably be detected is roughly given by the total length of the time series (from first to last datapoint), which is 12-13 days in the WFI runs. Nights with very few datapoints (≤ 5 , see Table 1) are unlikely to extend the baseline; excluding those nights gives $P_{\max} = 1.3 d$ for run A and 6 d for run C.

For a more realistic estimate of the sensitivity, we carried out simulations following the recipe given in Scholz & Eislöffel (2004b). In short: Non-variable objects were selected from our database. Sine-shaped periodicities with periods ranging from 1 to 200 h were added to their lightcurves. The noise level of the test objects and the amplitudes of the artificial periods were chosen to approximately reproduce the typical properties of the periods listed in Table 3. We then applied the algorithm described in Sect. 4.1 to these lightcurves and aimed to recover the imposed periods.

Fig. 5 shows the results for these simulations for runs A and C. The deviation between the imposed period and the detected period is negligible for $P < 10 h$, confirming that our period search is optimal for this range of periods. For $P = 10 \dots 90 h$ there are certain period ranges (e.g., around 24 h) for which we are unable to obtain reliable detections. In many cases, these ranges are narrow (typically $\delta P < 0.5 h$),

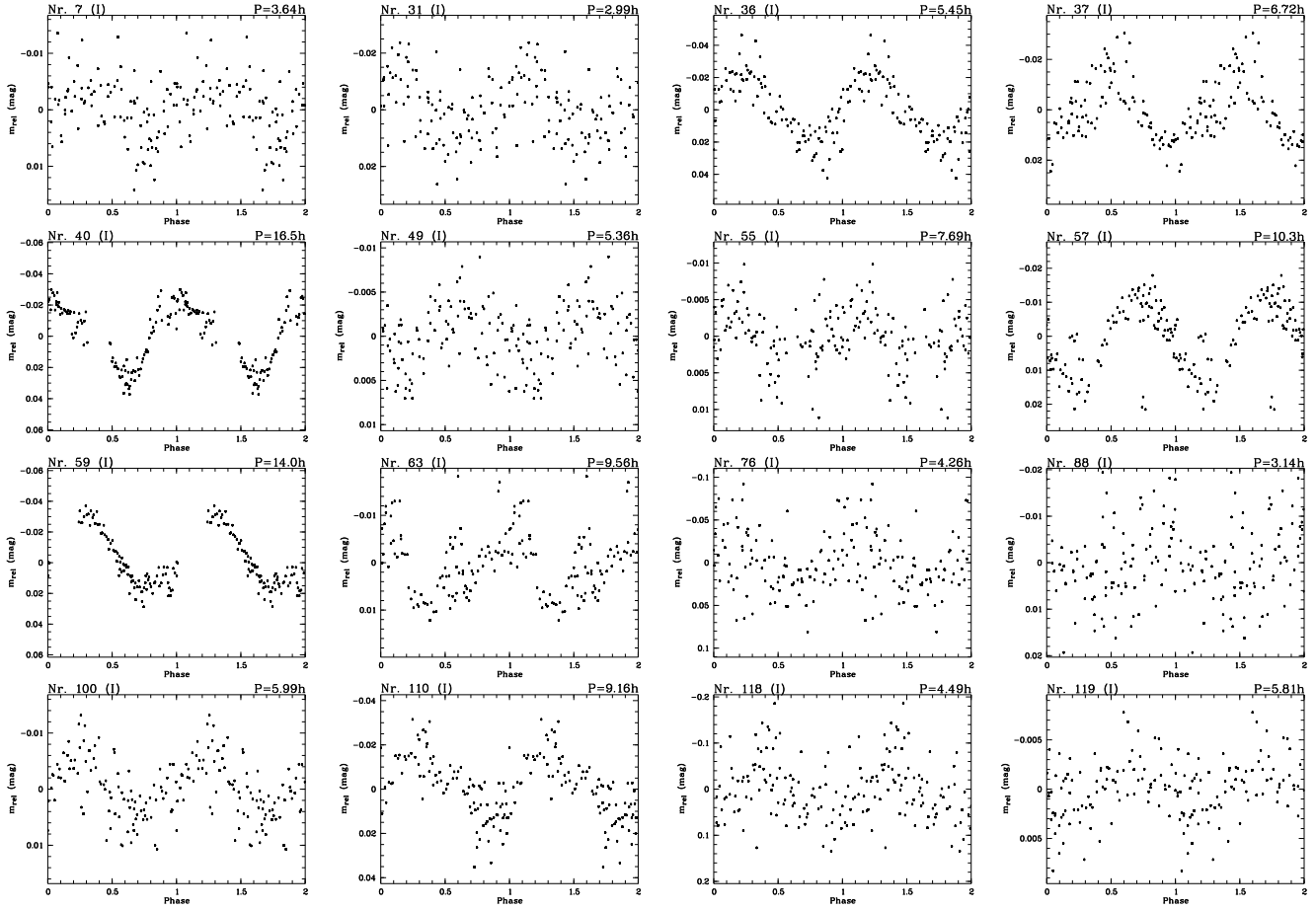


Figure 3. Phased lightcurves for the periodic objects from run A. Object id and photometric period are indicated.

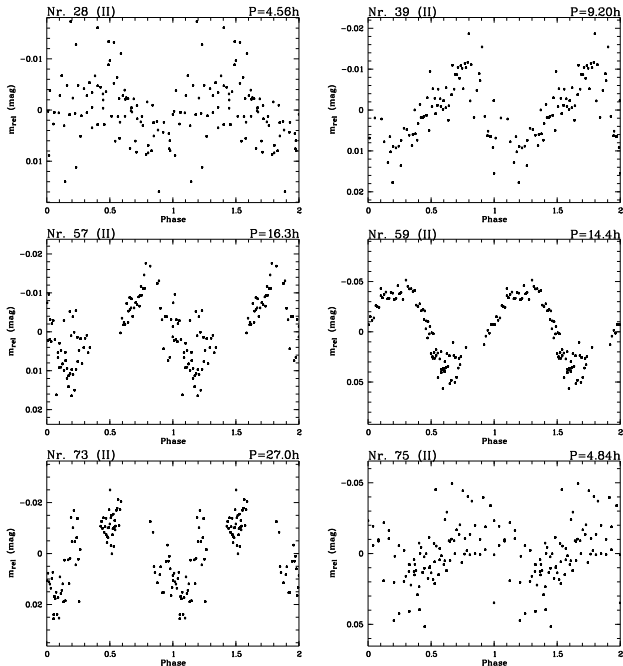


Figure 4. Phased lightcurves for the periodic objects from run C. Object id and photometric period are indicated.

particularly for run C. The plots clearly demonstrate that there are wide ranges of periods > 10 h in which our time series analysis is sensitive. For example, in run A we recover most periods with $P = 40 \dots 60$ h, and in run C we reliably recover $P = 50 \dots 62$ h and $P = 65 \dots 90$ h. There are only negligible windows of sensitivity for $P > 95$ h, which we identify as our upper period detection limit. The non-existence of any significant periods with $P > 30$ h in our candidate lightcurves thus points to a genuine lack of such objects in IC4665 (see Sect. 6).

4.2 The TLS lightcurves (run B)

While the photometry from runs A and C comes with similar noise characteristics, run B suffers from a comparatively small dynamic range and increased noise level, see Fig. 1. This hampers a direct comparison between the three runs. Instead of carrying out a time series analysis for all candidate lightcurves from run B, we use these time series to verify the periods reported in Table 3.

Out of 20 objects which are periodic in at least one of the WFI runs, 15 are bright enough to be detected in the TLS images. Nine out of these 15 do not show a significant period according to our tests. For the two objects #55 and #39 we confirm the periods listed in Table 3 within ± 0.1 h. For two objects we find periods at odds with the ones detected in the WFI runs: Object #63 has a 7.7 h period (run

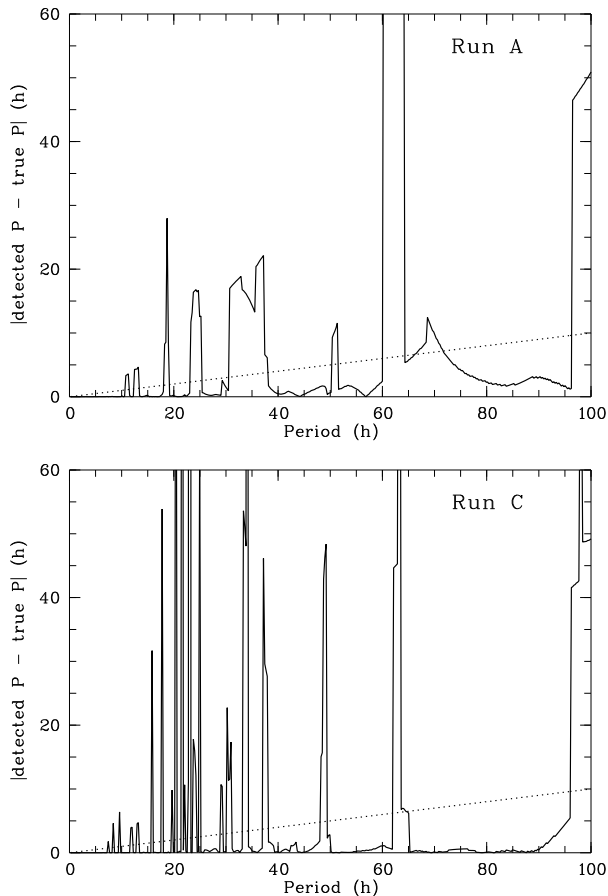


Figure 5. Results of the simulations to test the sensitivity in the period search. Plotted is the difference between imposed and detected period vs. the period for runs A (upper panel) and C (lower panel). The dotted line corresponds to a deviation of 10%.

A: 9.6 h), object #100 a ~ 110 h period (run A: 6.0 h). The latter case could indicate a long-term trend in the lightcurve on timescales of > 4 d and thus not detectable in the WFI runs. For both ambiguous cases, we re-checked the WFI periods and found them to be more convincing.

Of particular interest are the two objects for which both WFI runs yielded a period detection. For candidate #57 the best periods from the WFI campaigns are 10.3 h in run A and 16.3 h in run C. In both cases, however, the periodograms (Scargle and CLEAN) do exhibit a weaker, but still significant peak at the period found in the other run, respectively. The two possible periods are neither harmonics ($P_1 = nP_2$) nor beat periods ($1/P_1 = 1/P_2 + n$). In run B, this object is again variable with a period of 18.4 h, which is a clear beat period of 10.3 h, the period from run A (with $n = -1$). Thus, $P = 10.3$ h is the only period consistent with all three time series and is adopted as the most likely rotation period for this object in the following sections. The fact that the most significant period in dataset C differs from our consensus period, illustrates the difficulties of assigning periods to individual objects based on a single monitoring run. Due to the incomplete sampling in ground-based data, the lightcurve for a given object can sometimes be fit by more than one convincing period. This can be overcome with multiple observing runs, as demonstrated here.

Object #59 shows a period of 14.0 h in run A and 14.4 h in run C. The candidate is clearly variable in run B: Its lightcurve shows a gradual brightening of ~ 0.04 mag over the five nights. In addition, in night 5 the lightcurve exhibits several outlying datapoints which are 0.05–0.2 mag brighter than the average trend, but do not show the typical characteristics of a flare (see Sect. 4). For comparison, the average noise level for objects with similar brightness is 0.015 mag. However, we do not find any significant period in the lightcurve. In particular, the ‘consensus’ period of ~ 14 h obtained from the WFI lightcurves is not detected. Thus, while the variability of this object is confirmed, the period is not.

5 MAGNETIC SPOTS ON VERY LOW MASS OBJECTS

We found periodic variability for 20 likely VLM members of IC4665. The best explanation for this type of variability is the presence of surface features, co-rotating with the objects and thus modulating the flux, as it is usually assumed in monitoring studies for this type of targets. Alternative interpretations include pulsations and eclipsing binaries, but both are unlikely for our sample: a) Eclipsing binaries are simply too rare to be responsible for a significant fraction of our periodic objects. b) There is no evidence which points to pulsation in young M dwarfs with the periods observed in this study. All further discussions are based on the assumption that with the periodicities we indirectly observe surface features.

In our observations, the surface features causing the periodicities are almost certainly magnetically induced cool spots, simply for the lack of an alternative plausible scenario. It has been suggested that the condensation of dust molecules will form ‘clouds’ in substellar objects, which could in principle account for periodic variability as well. Our young targets, however, are not yet cool enough for this to happen. Models predict that dust condensation becomes relevant at $T_{\text{eff}} < 2500$ K (Helling et al. 2008), while the coolest objects in the sample given in Table 2 are likely to have $T_{\text{eff}} > 2700$ K. Moreover, our targets are expected to be mid to late M dwarfs, a spectral range known for strong magnetic activity. Thus, by analysing the lightcurves from our monitoring campaigns, we can put limits on properties of magnetic spots on VLM objects.

It is useful to recapitulate the conditions required to detect a photometric rotation period. Amplitudes and lightcurve shape will be influenced by the distribution of the spots on the surface. A degree of asymmetry in the distribution is required to cause a photometric period, but a slight deviation from symmetry would be sufficient to explain the small amplitudes seen in this study. Moreover, low-latitude spots are more relevant than polar spots for the lightcurve appearance.

The spot coverage (usually measured as filling factor) and temperature contrast (difference between photospheric and spot temperature) affect the amplitude of the photometric variability and thus the ‘success rate’ in monitoring campaigns. As shown in Scholz et al. (2005), both parameters are degenerate and cannot be determined separately based on single-filter lightcurves. Under the limiting assump-

tion that the spot temperature is $T = 0$ K, we can define a lower limit for the spot coverage: In that case, amplitudes of 1-10%, as seen in our period sample, would require a spot filling factor of at least 1-10%. In reality, the temperature contrast between photosphere and spots is more likely to be in the range of 100-1000 K (Scholz et al. 2005), implying more spot coverage than in the limiting $T = 0$ K case.

Finally, the inclination of the rotation axis against the line of sight will affect the lightcurve. For objects seen face-on, we expect flat lightcurves, independent of the spot properties. Assuming that the orientation of rotation axes in open clusters are randomly distributed, this will lower the fraction of objects with observed periodicity by a constant factor.

5.1 Spot activity vs. mass

The periods measured in Sect. 4.1 provide us with two indicators to assess the level of spot activity in our sample, the amplitudes and the fraction of objects with periods. The photometric amplitudes found in our period sample are ≤ 0.05 mag in the clear majority of the cases (20 out of 22), indicating that VLM objects in IC4665 show only low-level photometric variations. This is also reflected in the rms of their lightcurves, as discussed in Sect. 4 (see Fig. 1). Assuming that the contamination rate is similar in the total candidate sample and in the periodic sample, the fraction of objects with periods is 18% (20 out of 113). This number increases to 25% (20 out of 80), if we assume that the periodic objects have zero contamination (see Sect. 3).

These two results will now be compared with the outcomes of variability studies for more massive stars to test if spot activity changes with object mass. As comparison samples we mostly focus on four clusters with similar age, IC4665 itself, IC2602, α Per, and the Pleiades. Monitoring campaigns in these clusters were mostly carried out in the V-band, instead of the I-filter we have used. Assuming typical properties of cool spots, the photometric amplitudes are likely to be a factor of 1.5-2 larger in the V-band (Scholz et al. 2005). This has to be taken into account when comparing amplitudes from different authors.

In IC4665 Allain et al. (1996) monitored 15 F-K dwarfs and find 8 with period with amplitudes 0.01-0.1 mag, a 'detection rate' of 53%, significantly higher than in our campaigns. Barnes et al. (1999) observed all spectroscopic members of IC2602 and measured periods for 29 out of 33 F-K dwarfs, a fraction of 88%. With one exception, all amplitudes are ≤ 0.08 mag. In the α Per cluster Prosser et al. (1993) and O'dell & Collier Cameron (1993) find photometric periods for $\sim 90\%$ of the monitored F-K stars with typical amplitudes ≤ 0.1 mag. In all these studies, the range of amplitudes is similar to our lightcurves, particularly after converting from V- to I-band. The detection rate, on the other hand, is 50-90% and thus clearly higher than in our VLM sample.

The main observational selection effects that might influence the period detection rates are photometric accuracy, sampling of the time series, and a biased choice of targets. The photometric accuracy in our campaigns (particularly runs A and C) is better than in most aforementioned literature studies. In addition, most of the literature studies rely on fewer datapoints and are probably less sensitive to short

periods. Combining both effects, we would expect to find a larger fraction of periodic objects, not the opposite.

All our targets are selected from photometry alone and are thus unbiased with respect to the rotation/activity properties. To our knowledge, the same applies to the samples observed in Allain et al. (1996) and Barnes et al. (1999). The α Per samples might be biased towards fast rotating objects, since O'dell & Collier Cameron (1993) selected presumed fast rotators for their monitoring study. Since the rotation-activity relation for periods of 1-5 d is flat in these clusters (Patten & Simon 1996), this does not imply a bias in activity levels. Overall, selection effects do not appear to be responsible for the low number of stars with period in our sample. More likely, this finding is caused by a mass dependence in the spot properties.

Monitoring studies in NGC2264 (Lamm 2003; Herbst et al. 2007) and in the Pleiades (Scholz & Eislöffel 2004b) have pointed at a drop in photometric amplitudes by a factor of about 2 in the very low mass regime. This has been interpreted as evidence for a change in spot properties at $M \sim 0.3 - 0.5 M_{\odot}$. We cannot confirm this drop in amplitudes in IC4665, which may be due to the small sample size. Indirectly, however, we confirm these findings, as low amplitudes could prevent period detection.

Possible explanations for low amplitudes and/or a low fraction of periodic lightcurves are a) very few spots, b) low contrast between spots and photosphere, c) many symmetrically distributed spots or one polar spot. From multi-filter monitoring Scholz et al. (2005) conclude that a) and/or c) are the most plausible scenarios. We note that the current results from Zeeman Doppler imaging point towards large-scale, poloidal fields for fully convective very low mass objects (Morin et al. 2008b). This indicates the presence of large polar spots and a lack of spots at low latitudes, which reinforces hypothesis c).

5.2 Long-term spot evolution

With our three monitoring campaigns covering three years, we are for the first time able to probe the long-term evolution of magnetic spots in VLM objects. Of particular relevance is the comparison between the two WFI time series (run A and C): Having similar noise characteristics and sampling, they allow us a direct check for long-term variations in the lightcurve.

The most important finding here is that out of 20 objects with detected period, only two show a period in both campaigns. The lightcurves of those two objects will be further discussed in Sect. 5.3. In the majority of the cases, the characteristics of the spots have changed sufficiently after three years, preventing the confirmation of the period. Persistent spot activity is thus a rare phenomenon in young VLM objects.

This result can again be compared with the properties of more massive stars. Large samples of solar-mass stars at ages 1-5 Myr have been monitored repeatedly in the past, allowing us to put constraints on the stability of the spot activity. Cohen et al. (2004) have published a five-year study of T Tauri stars in IC348. In agreement with other studies (e.g. Nordhagen et al. 2006), they find variations in amplitude and lightcurve shape between different seasons. In their sample, 14 out of 27 stars with periodic variability exhibit

Table 4. Results from the period fitting to the lightcurves for objects #57 and #59. The period error ΔP (h) has been determined following Horne & Baliunas (1986). The period fit did not yield significant results for the run B lightcurves; the periods from that run are considered unreliable.

ID	run	P (h)	ΔP (h)	A (mag)
57	A	9.99	0.04	0.026
	B	10.45	–	0.017
	C	9.69	0.04	0.017
59	A	14.04	0.04	0.047
	B	13.17	–	0.027
	C	14.45	0.04	0.083

the period in all five seasons; 23 of 27 stars in at least two out of five seasons. This is consistent with results from work in the Orion Nebula Cluster, where Rebull (2001) finds that about half of the periods measured in 1996/97 can be recovered in a dataset obtained about a year earlier, although this earlier run had more ‘patchy’ sampling. Spot stability over several years has also been inferred from Doppler imaging studies (e.g. Vogt et al. 1999).

Thus, for young solar-mass stars about half of the objects retain a detectable period over more than one season. In contrast, only 10% of the VLM objects in IC4665 exhibit a photometric period in both WFI campaigns separated by three years. This again points to a change in the spot properties in the VLM regime, as discussed in Sect. 5.1. In very low mass objects, spot activity causing photometric variability on the percent level is rare and transient. Since the amplitudes in our sample are small and in many cases close to the photometric noise limit, only a slight change in lightcurve amplitude, caused for example by a re-configuration of the spots, could lead to a non-detection in the period search. Thus, the lack of objects with stable periods may be a direct outcome of the drop in amplitudes in the VLM regime.

5.3 Objects with persistent periodic variability

The two most interesting objects in our sample are probably candidates #57 and #59, both with persistent periodic variability in all three observing campaigns, spanning three years. With masses $\sim 0.2 M_{\odot}$ these two objects belong to the lowest mass stars known to date with long-term photometric variability. They are thus prime targets for follow-up studies, e.g. multi-filter monitoring or Doppler imaging.

We re-determined the periods for #57 and #59 by fitting sine functions to the lightcurves from each run. The free parameters in the fit are phase, amplitude, and period, but the period was restricted to a small range around the assumed rotation period of 10 and 14 h, respectively (see Sect. 4.2). The fit results are summarised in Table 4. We do not attempt to fit all three seasons with a single periodic function, because the period uncertainty accumulated over a year or more causes a phase uncertainty larger than the period itself. In Fig. 6 we show for both objects the three lightcurves phased to the period given in Table 4. As pointed out earlier, the rotation periods are not recovered in run B, but for object #57 the beat period at 18.6 h is detected. The period fit for run B are thus not considered trustworthy.

In the following, we will discuss change in amplitude, lightcurve shape, and period over the three seasons. For object #57 the photometric amplitude is constant within the errorbars over all three seasons. For object #59, however, the amplitude shows striking variations: It drops by a factor of about two from 1999 to 2001 and increases then by a factor of about three between 2001 and 2002. The two most likely scenarios for such changes are a re-configuration of the magnetic spots and a strongly variable spot filling factor.

For both objects, the shape of the lightcurves are in good agreement with the sine function. This is not particularly surprising since the periods have been determined by trying to match a sine curve. The more relevant result is that the shape of the lightcurve does not change significantly over the three seasons. For object #59 this is demonstrated in Fig. 7: We plot the datapoints from run A and run C in phase to the period measured for run C (14.45 h) scale the lightcurve from run A by a factor of 1.766 to match the amplitude of run C, and overplot them with the lightcurve measured in run C.

As can be seen in this plot, both sets of datapoints cover the same regions in phase space. The deviations between both lightcurves are fully consistent with the expected scatter of about ± 0.015 mag, given as solid lines in Fig. 7. This noise estimate includes the combined photometric noise of both campaigns (~ 0.01 mag), uncertainty in the period, and possible other sources of variability (e.g., microflares). Thus, within the uncertainties the lightcurves from run A and C are identical, except for a clear change in amplitude. Since any re-configuration of the magnetic spots is expected to alter the shape of the lightcurve, this favours a variable spot filling factor as explanation for the change in amplitude, maintaining the magnetic configuration constant. Assuming that spot temperatures are on average constant, changes in the spot coverage by a factor of 2-3 on timescales of years are required to match the observations.

Magnetic cycles, as seen in solar-type stars, are one possible reason for a long-term variation in the spot filling factor. As of today, simulations of the magnetic field generation do not find strong evidence for the presence of cycles in fast rotating fully convective objects (Chabrier & Küker 2006; Dobler et al. 2006; Browning 2008). Our result might pose a challenge to these models and certainly motivates continued monitoring of variable VLM stars.

In principle, our long-term study also allows us to probe differential rotation: If the rotation rate is a function of latitude, we expect to measure small changes in the rotation periods in different seasons, depending on the latitude of the dominant spot group. The rate of differential rotation can then be estimated simply from the scatter of the measured rotation rates $\Delta\omega$. Our candidates #57 and #59 show period changes of 0.3 and 0.4 h between run A and C. This translates to $\Delta\omega$ of 0.4 rad d^{-1} for object #57 and 0.3 rad d^{-1} for object #59, corresponding to 2-3% of the rotational velocity.

The formal errors from the period fit are smaller than that (0.04 h), which would indicate a detection of significant differential rotation in those two objects. A more detailed look on the lightcurves, however, shows that the actual uncertainties in the period measurement are likely to be larger: Due to the lack of datapoints outside two consecutive nights, the periodogram peaks for run A are broad enough to allow for period uncertainties of ~ 0.5 h. More specifically, the pe-

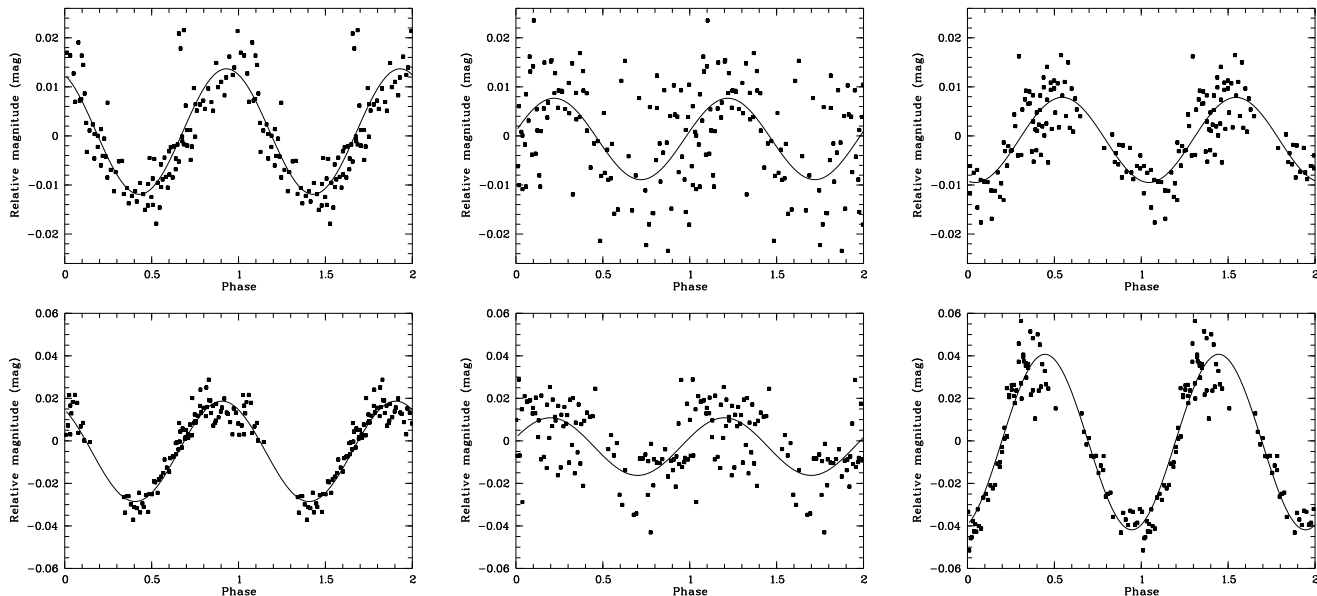


Figure 6. Phaseplots for objects #57 (upper panels) and #59 (lower panels) for runs A to C (from left to right). The lightcurves are plotted in phase to the assumed rotation period of ~ 10 h and ~ 14.2 h, respectively. The best-fit sine function is overplotted, see Table 4 for the fit parameters. Note the changing y-axis scale in the 3rd panel in the lower row.

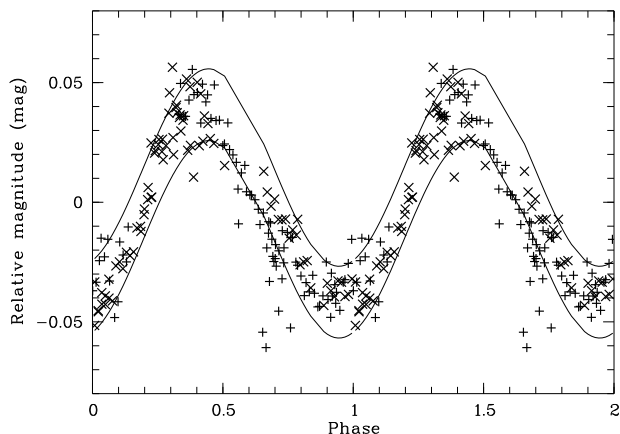


Figure 7. Combined datapoints from run A (plusses) and C (crosses) for object #59. Both lightcurves are plotted in phase to the period measured in run C (14.45 h). The lightcurve from run A has been scaled by a factor of 1.77 to match the amplitude in run C. The two solid lines give the range expected from the 1σ photometric noise.

riods obtained for run C give a convincing (albeit not the best) fit to the lightcurves from run A. Therefore, we consider the periods from run A and C to be consistent for both objects, and treat the period differences as upper limits for the rate of differential rotation.

From theoretical ground, fully convective objects are expected to show only little, if any, differential rotation (Chabrier & Küker 2006; Dobler et al. 2006; Browning 2008). Monitoring campaigns on T Tauri stars have confirmed this prediction (Cohen et al. 2004; Herbst et al. 2006), with period changes rarely exceeding a few percent. For VLM objects there is growing evidence that the differential rotation rate is negligible, as found by Doppler imaging

($< 0.05 \text{ rad d}^{-1}$, Barnes et al. 2005) and Zeeman Doppler Imaging ($\sim \text{mrad d}^{-1}$, Morin et al. 2008a,b). Our findings in IC4665 are certainly consistent with the expectations. Given the lack of objects with persistent variability in this mass regime, it is challenging to derive more stringent limits on differential rotation from photometric monitoring alone.

6 ROTATION PERIODS IN IC4665

As established in Sect. 5, the observed photometric periods correspond to the rotation periods of our targets.² The sample of 20 new rotation periods for likely VLM members in IC4665 increases the number of objects with known periods in this cluster by a factor of three. In Fig. 8 we plot the total sample of published periods in IC4665 as a function of mass, including our own periods and the results from Allain et al. (1996) for F-K stars in this cluster. We note that the Allain et al. (1996) variability campaign is likely not highly sensitive to very short periods (< 10 h), due to a small number of datapoints per observing night.

The main feature in Fig. 8 is the cumulation of our datapoints at periods < 1 d, or conversely the distinct lack of slow rotators in the VLM regime. Our period search may be incomplete, but it is definitely sensitive for periods up to 4 d, as discussed in Sect. 4.1. Thus, the observed lack of slow rotators in the VLM regime is not induced by our sampling. This finding is supported by period samples in other young clusters – VLM objects are almost exclusively seen as fast rotators, with the exception of objects with ages < 5 Myr, when disk-star interactions might still play a role. The data

² In rare cases, a particular spot distribution might generate a photometric period which is half the rotation period, e.g. when two similarly large features are located at opposite latitudes.

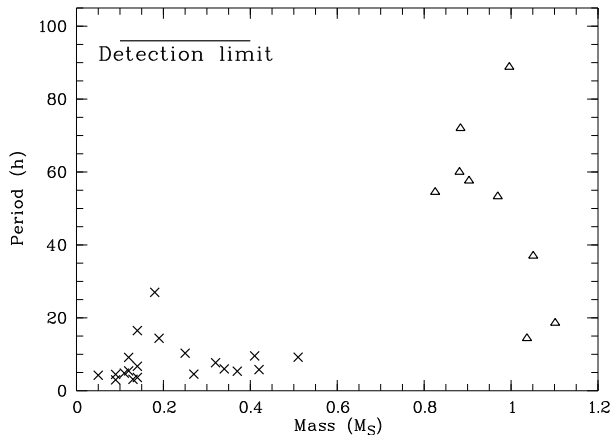


Figure 8. The total sample of rotation periods in IC4665, plotted vs. object mass. Crosses are periods from this paper for VLM objects, triangles show periods from F-K stars (Allain et al. 1996). The horizontal line in the top left corner indicates the approximate detection limit in our period search. All mass estimates have been derived in a consistent way and are thus comparable.

in IC4665 provide another piece of evidence for a strong rotation-mass dependence.

To date we have no evidence that there is a population of slowly rotating VLM objects not found in the period searches. For the age and mass range considered here, photometric amplitudes are observed to be more or less independent of rotation, without any drop-off at long periods (Irwin et al. 2008b), which could cause us to miss long periods. We note that Irwin et al. (2009) do in fact report such a drop-off for stars with $0.5 < M < 1.1 M_{\odot}$, age 130 Myr, and $P > 10$ d. We do not attribute too much relevance to this result in the context of the current study, for three reasons: a) The mass range and age are not comparable with our targets. b) Our study is focused on the period range < 4 d, for which no drop-off in the amplitudes is reported. c) There is independent evidence for an upper period limit well below 10 d in the VLM regime.

This evidence comes from the available $v \sin i$ data obtained by high-resolution spectroscopy, which is not biased with respect to the spot activity. Albeit based on a limited sample, the lower envelope of $v \sin i$ in the Pleiades (120 Myr) for $M < 0.4 M_{\odot}$ is well defined (Terndrup et al. 2000). In Scholz & Eislöffel (2004b) we have shown that it translates into an upper limit for the rotation periods of 1-2 d, in good agreement with the available periods in the Pleiades as well as in IC4665. Thus, the observed lack of slow rotators likely is a genuine effect and affects *all* VLM objects, and not only the ones with detected period.

In the following subsections we discuss rotation in the VLM regime. In Sect. 6.1 we focus on our new periods and evaluate the pre-main sequence rotational evolution based on the currently available data. We find clear evidence for rotational braking on timescales of 5-50 Myr. In Sect. 6.2, we review the currently used wind braking laws for stars and brown dwarfs, before applying them to pre-main sequence data in Sect. 6.3. Finally, we put these results in context and identify problems and future directions for research on rotation and magnetic properties (Sect. 7).

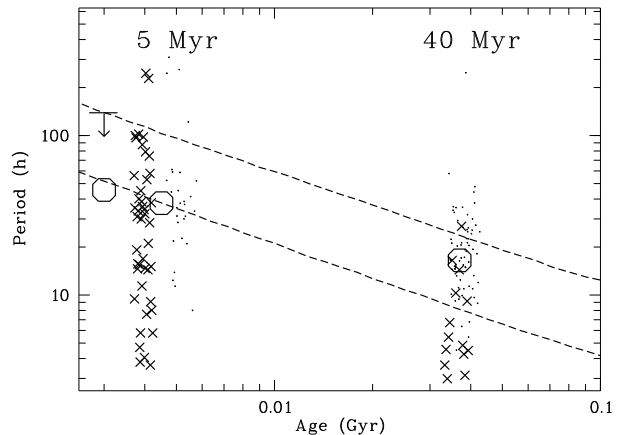


Figure 9. Rotational evolution of VLM objects in the pre-main sequence phase. Plotted are periods for objects with $M < 0.3 M_{\odot}$ in the clusters σ Ori and ϵ Ori (average age ~ 4 Myr, Scholz & Eislöffel 2004a, 2005), NGC2362 (age ~ 5 Myr, Irwin et al. 2008a), IC4665 (this work), and NGC2547 (age ~ 38 Myr, Irwin et al. 2008b). The period data for any given cluster is plotted at a range of ages scattered randomly around the most likely cluster age, for clarity. The large polygons show the median period for $0.1 < M < 0.3 M_{\odot}$. In addition to the groups of clusters at 4-5 and ~ 40 Myr, we plot median and 90%-ile for VLM objects in NGC2264 at ~ 3 Myr (Lamm et al. 2005, $M < 0.25 M_{\odot}$ on their mass scale). The dashed lines show the period evolution assuming angular momentum conservation based on the evolutionary tracks by Baraffe et al. (1998) for $0.3 M_{\odot}$ (upper track) and $0.2 M_{\odot}$ (lower track).

6.1 Tracing the pre-main sequence evolution

There is now a substantial sample of rotation periods for VLM objects in young open clusters. With at least 20 VLM periods in seven pre-main sequence clusters (ONC, NGC2264, σ Ori, ϵ Ori, NGC2362, IC4665, NGC2547) we are in a position to put firm limits on the rotational braking at very young ages (see Herbst et al. 2007; Irwin et al. 2008b). In Fig. 9 we plot periods for objects with $M < 0.3 M_{\odot}$ as function of cluster age. As crosses we show periods in the clusters σ Ori (Scholz & Eislöffel 2004a), ϵ Ori (Scholz & Eislöffel 2005) – both plotted at an approximate age of ~ 4 Myr –, and IC4665 (this paper, age ~ 36 Myr). Periods from the *Monitor* project are plotted as small dots, for the clusters NGC2362 (age ~ 5 Myr, Irwin et al. 2008a) and NGC2547 (age ~ 38 Myr, Irwin et al. 2008b). In total, we base the following discussion on 72 periods at 4 – 5 Myr and 82 periods at ~ 40 Myr.

For the youngest clusters in this plot, the fraction of objects with disks and/or accretion is $< 10\%$, thus rotational braking due to disk/star interaction is not relevant here. In all five clusters, the object masses have been determined in a consistent way, thus the cut-off at $0.3 M_{\odot}$ is consistently defined for all ages. For completeness, we also plot the median and the 90%-ile of the VLM periods in NGC2264 at age of 3 Myr (Lamm et al. 2005), noting that both masses and ages in this cluster are probably not fully comparable with the remaining datasets.

The monitoring campaigns in Orion and IC4665 are deeper than the *Monitor* data, extending into the substellar regime. Combined with the well-established period-mass

relation in the VLM regime, this explains the fact that the period samples in these clusters extend to shorter periods. The upper period limits, however, are defined by the highest mass objects in those samples and thus comparable. To probe the evolution for a typical VLM star, we plot the median period for objects with $0.1 < M < 0.3 M_{\odot}$ as large polygons, a mass regime where all variability campaigns are sensitive. For this purpose we join the samples at similar ages, i.e. Orion and NGC2362 (median 37.7 h, based on 57 objects) as well as IC4665 and NGC2547 (median 16.5 h, based on 78 objects).

The two dashed lines in Fig. 9 provide the comparison with the theory. They show the calculated rotational evolution assuming angular momentum conservation ($P(t) = P_0 \times (R(t)/R_0)^2$). Both tracks are based on the radii from the Baraffe et al. (1998) evolutionary tracks for solar-metallicity stars. The upper track is for a $0.3 M_{\odot}$ star and can thus be compared with the upper period limit, while the lower track is for a $0.2 M_{\odot}$ star, meant to provide a comparison with the median values.

Comparing periods and model tracks clearly shows that the observations are not in agreement with angular momentum conservation at timescales of 5-50 Myr. The expected median period for a VLM star at ~ 40 Myr is about 8 h, while the observed median is approximately twice as high. Similarly, the upper period limit at 40 Myr is not well-represented by the model: The track starts at $P_0 \sim 100$ h, with only 6 objects ($8 \pm 3\%$) have periods exceeding this value at young ages. At ~ 40 Myr, however, 24 out of 82 objects ($29 \pm 5\%$) exceed the predicted period of ~ 22 h. Excluding the highest 8% of the periods at 40 Myr yields an upper limit of about 36 h, a factor of 1.6 too high compared with the prediction for angular momentum conservation.

In summary, rotational braking clearly occurs for objects with masses of 0.1 - $0.3 M_{\odot}$ on timescales of ~ 50 Myr. We see an offset between prediction for angular momentum conservation and observed periods by a factor of 1.6–2, implying a reduction in angular momentum by 40-50% compared with the case without any braking. Note that this effect can hardly be explained by uncertainties in the radii from the Baraffe et al. (1998) models: We only use the ratio of radii at different ages, thus any systematic problem with the models is likely to be eliminated. Moreover, radii from these models are found to be in good agreement with observations for early/mid M dwarfs (Mohanty et al. 2004; Scholz et al. 2007).

6.2 Wind braking in stars and brown dwarfs

Stellar winds powered by magnetic fields are the main physical process governing the rotational braking on long timescales. Angular momentum losses due to stellar winds are commonly modeled based on the parameterisation by Kawaler (1988), which is derived from the analytical wind braking law by Mestel (1984):

$$\frac{dJ}{dt} = -K\omega^{1+4aN/3} \left(\frac{R}{R_{\odot}}\right)^{2-N} \left(\frac{M}{M_{\odot}}\right)^{-\frac{N}{3}} \left(\frac{\dot{M}}{10^{-14}}\right)^{1-\frac{2N}{3}} \quad (1)$$

Here N is the 'wind index' describing the topology of the magnetic wind and a is the dependence of the magnetic field on the rotation rate, $B \propto \omega^a$ (Barnes & Sofia 1996).

In most studies, a value of $N = 1.5$ is chosen, corresponding to a mixture between dipole ($N \sim 0.5$) and radial ($N = 2.0$) field. By adopting $a = 1.0$ and thus a linear relation between B-field and rotation rate, one obtains $dJ/dt \propto \omega^3$ and reproduces the Skumanich law $\omega \propto t^{-1/2}$, the empirical relationship for the decay of rotation rates of G-type stars on the main-sequence (Skumanich 1972).

This particular choice of the parameter a , however, fails to be applicable to the 'ultra-fast rotators' (UFRs) in young open clusters. In addition, it does not take into account that magnetic activity indicators are observed to saturate at high rotation rates (see Patten & Simon 1996, and references therein). Therefore, it is usually assumed that the magnetic field saturates at a critical rotation rate, i.e. $a = 0.0$ for $\omega > \omega_{\text{crit}}$. With the same wind index as in the Skumanich case, Equ. 1 then yields $dJ/dt \propto \omega_{\text{crit}}^2 \omega$ and $J(t) \propto \exp(t/\tau)$, with $\tau = 1/\omega_{\text{crit}}^2$. By scaling ω_{crit} appropriately with mass or effective temperature, models using this bimodal parameterisation of the angular momentum losses are indeed able to reproduce the main features in the available rotation period (e.g. Bouvier et al. 1997; Sills et al. 2000; Irwin et al. 2006) and $v \sin i$ data (e.g. Terndrup et al. 2000; Reiners & Basri 2008).

Introducing a scaling of the critical rotation rate with mass or convective turnover timescale is justified, because the magnetic field generation is unlikely to be comparable in stars with different interior structure. Main-sequence stars with spectral types F to early M possess a radiative core and a convective envelope. The convection zone becomes progressively deeper with decreasing mass, so that all VLM objects are fully convective throughout their evolution. These changes are likely to have consequences for the dynamo processes generating the stellar magnetic fields. For example, it has been suggested that fully convective objects host an α^2 dynamo (Chabrier & Küker 2006) or a distributed dynamo (Durney et al. 1993) instead of the solar-type $\alpha\omega$ dynamo. Barnes (2003b) proposed that the saturated ($a = 0.0$) and linear regimes ($a = 1.0$) of the angular momentum loss law represent objects with 'convective' and 'interface' magnetic fields, called objects on the C-sequence or I-sequence. For consistency reasons, we will use this nomenclature in the following.

6.3 Application to pre-main sequence objects

Pre-main sequence VLM stars with ages between 10 and 100 Myr are almost exclusively fast rotators and are thus considered to be on the C-sequence with $\omega > \omega_{\text{crit}}$ (Pizzolato et al. 2003). The e-folding timescale for their wind braking is probably > 1 Gyr (Delfosse et al. 1998; Scholz & Eislöffel 2007); the angular momentum losses on the pre-main sequence depend primarily on radius with $\omega \propto R^{3/2}$, according to Equ. 1. This gives an angular momentum loss of $\sim 30\%$ on timescales of 50 Myr. As evaluated in Sect. 6.1, observations indicate losses of 40-50%. Taking into account uncertainties in cluster ages and spin-down timescale as well as the fact that a few objects might

experience additional braking by star-disk interaction, this agrees well with the prediction.³

On the other hand, the observed estimates of angular momentum losses in the VLM regime are nowhere near the effect expected for the I-sequence. Skumanich braking gives angular momentum losses of $> 70\%$, i.e. significantly larger than the values seen in the VLM regime. This simply confirms that VLM stars on the pre-main sequence have to be considered objects on the C-sequence. In summary, the rotational data for pre-main sequence VLM objects, including our new periods in IC4665, fit the current paradigm for the rotation evolution, as described in Sect. 6.2.

In Scholz et al. (2007), $v \sin i$ for F to early M stars in young stellar associations with ages between 6 and 30 Myr have been analysed, a dataset that is complementary to the periods shown in Fig. 9. Similarly to the VLM objects, the rotational pre-main sequence evolution of solar-mass stars is incompatible with Skumanich braking and allows only for relatively little angular momentum loss. Thus, in the pre-main sequence phase all stars seem to go through a C-sequence phase of rapid rotation and weak wind braking. They make the transition to the I-sequence and thus 'switch on' the Skumanich braking at an age t_{C-I} , which is a function of mass. This has also been suggested in a recent paper by Meibom et al. (2009). According to the current data, t_{C-I} is 50 – 100 Myr for $1.0 M_{\odot}$, 0.5-1 Gyr for $M = 0.5 M_{\odot}$ (Scholz & Eisloffel 2007), and several Gyrs for $M < 0.3 M_{\odot}$ (Delfosse et al. 1998). The transition between I- and C-sequence generates a large gap in rotation rates between solar-mass and VLM stars on the main sequence.

7 TWO REGIMES OF MAGNETIC PROPERTIES

In Fig. 10 we summarise the rotational evolution scheme described in the previous Sect. 6. This figure is meant to serve as a qualitative illustration and does not provide an accurate quantitative description. All stars start on the C-sequence with moderate wind braking in the pre-main sequence phase. At a given age t_{C-I} which is a function of mass they make the transition to the I-sequence with Skumanich type spindown. In Fig. 10, we plot the C-sequence in solid lines and the I-sequence in dashed lines. For t_{C-I} we assume 0.05 Gyr for $1 M_{\odot}$ and 0.5 Gyr for $0.5 M_{\odot}$, consistent with the currently available constraints (see Sect. 6.3). Additionally, we assume that the e-folding timescale τ on the C-sequence scales with object mass. We neglect here the dependence of the rotational braking on the radius, which is relevant in the pre-main sequence phase.

With the I- and the C-sequence two regimes of wind braking have been identified. In order to explore the underlying physics of these regimes, we look for differences in the magnetic properties between C- and I-sequence. The age sequence defined by the transition from C- to I-sequence is similarly seen in the fall-off of chromospheric H α emission, which occurs at ~ 50 Myr for G-K stars, at 0.5-1.0 Gyr for early M stars (Hawley et al. 1999), and at several Gyrs for

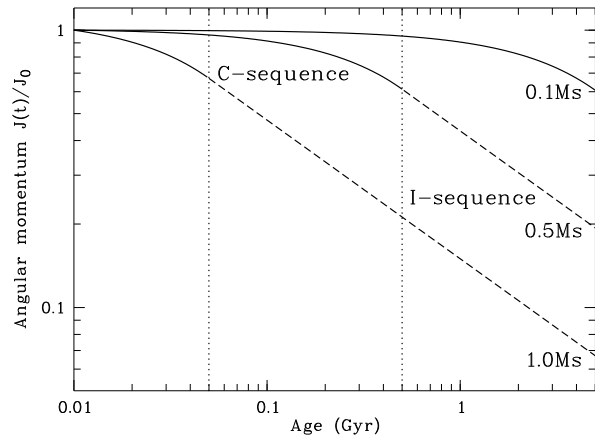


Figure 10. Schematic representation for the rotational evolution of stars at three different masses. Solid and dashed lines show the spindown on the C-sequence and I-sequence, respectively. The vertical dotted lines illustrate the transition from C- to I-sequence for $1 M_{\odot}$ (at 0.05 Gyr) and $0.5 M_{\odot}$ (at 0.5 Gyr). The effect of the pre-main sequence contraction has been neglected here (see text).

Table 5. Qualitative summary of observable properties for objects on the C- and I-sequence. For more references see text.

	C-seq	I-seq
rotation	fast	slow
MS wind braking	$\propto \exp(t)^a$	$\propto \sqrt{t}$
H α emission	yes ^b	no/weak
rotation/activity relation	flat ^c	linear
differential rotation	no/weak ^d	strong
magnetic topology	poloidal ^e	poloidal/toroidal
spot activity	weak ^f	strong

^a Barnes (2003b, and references therein)

^b e.g., Hawley et al. (1999, 2000)

^c e.g., Patten & Simon (1996)

^d Barnes et al. (2005); Morin et al. (2008a)

^e Donati et al. (2006); Morin et al. (2008a)

^f this paper

M3-M5 stars (Hawley et al. 2000). This may indicate that the onset of H α activity and the transition from C- to I-sequence are related, i.e. the 'switching on' of the Skumanich braking goes along with a drop in H α activity.

As already discussed in Sect. 6.2, the rotation/activity relation is flat for very young stars at 1 Myr (Stassun et al. 2004) and VLM objects (Mohanty & Basri 2003), both C-sequence objects, and linear for slowly rotating solar-mass stars on the I-sequence (see also Barnes 2003a). There are clear indications for a change of the magnetic field topology at the transition to fully convective objects (Donati et al. 2006). Additionally, the characteristics of the photometric lightcurve, caused by magnetically induced spots, change significantly in the VLM regime (see Sect. 5). Thus, C- and I-sequence are likely to constitute two different magnetic regimes. We summarise the currently available evidence for the bimodality in magnetic/rotational properties in Table 5.

In the parametrisation for the wind braking given in Sect. 6.2, two parameters determine if an object belongs to the C- or I-sequence: rotation rate and mass. Since both pa-

³ Note that the dependence on radius in the wind law has been neglected in various previous publications, e.g. Scholz & Eisloffel (2004b); Herbst & Mundt (2005).

parameters are interdependent, one of them may be of more fundamental relevance than the other. It is particularly tempting to explain the whole body of rotation/magnetic properties based exclusively on stellar mass, because it determines the interior structure, as pointed out in Sect. 6.2: While VLM objects and very young stars are fully convective, main-sequence F-K stars harbour a radiative core. This difference may be the fundamental reason for the two regimes of rotational/magnetic properties.

However, as already discussed in Scholz & Eislöffel (2007), the mass and age limits for the transition from C- to I-sequence do not coincide with the prediction for the occurrence of the radiative core; thus there is no clear-cut connection between the change in internal structure and the change in rotation/magnetic properties. For all objects that do not remain fully convective throughout their evolution (i.e. $M > 0.35 M_{\odot}$), the radiative core in F-K stars is thought to appear at $<10\text{-}30$ Myr and is fully developed after $<100\text{-}200$ Myr (Chabrier & Baraffe 1997; D’Antona & Mazzitelli 1994), significantly earlier than the transition from C- to I-sequence. To maintain the notion that internal structure is essential for magnetic properties, one has to assume that following the formation of a radiative core, it takes a considerable timespan before the characteristics of the I-sequence (see Table 5) become observable.

If interior structure is the underlying reason for the two regimes, VLM objects – fully convective throughout their evolution – are not supposed to leave the C-sequence. This is clearly at odds with the observations. Several studies have identified mid/late M dwarfs with very low or undetected $v \sin i$ and activity levels below the range expected for the saturated regime (Hawley et al. 2000; Mohanty & Basri 2003). Albeit fully convective, these VLM stars are likely to constitute the non-saturated regime, suggesting that slowly rotating VLM objects do exist and can operate an I-type (Skumanich) rotational braking. From these simple arguments it seems unlikely that interior structure (or mass) alone can account for the two different regimes of magnetic/rotational properties. Thus, two parameters, rotation and mass, are required to distinguish between I- and C-sequence.

The fact that we observe two regimes of magnetic properties points to a more general problem in the current models, as described in Sect. 6.2. The braking laws for I- and C-sequence both assume $N = 1.5$, a wind structure somewhere between dipole and radial field. By holding this parameter constant, it is implicitly assumed that all low-mass stars and brown dwarfs share the same type of magnetic field structure, with saturation on the C-sequence being the only difference. As outlined above, there is clear evidence for a change of magnetic field properties at the transition from C- to I-sequence (see Table 5), which makes the choice of constant N questionable. The specific benefit of the value $N = 1.5$ is that it conveniently cancels out the mass loss rate in the wind braking law, which is difficult to constrain by observations. On the other hand, the explanatory power of an angular momentum loss law that does not include the mass loss rate is probably limited.

For a more satisfying understanding of the underlying physics, it may be needed to re-investigate the parametrisation of the wind braking law in Equ. 1. For solar-mass stars, Barnes & Sofia (1996) originally proposed two ways to ex-

plain the ultrafast rotators in young open clusters, objects that we would classify as being on the C-sequence: either with saturation ($a = 0.0$ instead of 1.0) or with a low value for the wind index until 100 Myr ($N < 1$, close to a dipole field) and then switching to the Skumanich type $N = 1.5$. The second type of parametrisation has not been explored in detail and may turn out to be closer to the physical reality. While saturation of magnetic activity at high rotation rates is a well-established fact (see Patten & Simon 1996, and references therein), it is probably the filling factor that saturates (Saar 1996). When choosing $a = 0.0$ in the wind braking law, however, we assume that the magnetic field strength is saturated. It may be necessary to resort to models with a and N as free parameters, thus accommodating both for saturation and a change in the magnetic wind structure.

The choice of $N = 1.5$ may not be appropriate for the Skumanich type I-sequence either: Recent numerical simulations by Matt & Pudritz (2008) indicate a significantly smaller value for this parameter (about 0.7 instead of 1.5). This would imply that angular momentum losses depend at least weakly on the mass loss rate ($dJ/dt \propto \dot{M}^{0.5}$), which is probably a more plausible description than one without dependence on \dot{M} .

From these considerations it becomes clear that the currently available theoretical framework for the stellar spin-down is lacking a satisfactory description of the physics of the rotation-wind connection. Future work should aim to verify the bimodal wind braking law as given in Equ. (1) and explore possible alternatives. Observationally, the emerging problems encourage to obtain more reliable constraints on mass loss rates, as this may turn out to be crucial to improve the modeling of rotational evolution. Having said this, the bimodal schematic used in current models and described in detail above has been proven to have considerable predictive power. Given a proper calibration, it allows us to use rotation rates as indirect indicator of stellar ages and masses.

8 CONCLUSIONS

We have monitored a large sample of very low mass objects and brown dwarfs in the young cluster IC4665 over three seasons, aiming to measure rotation periods and to assess the long-term evolution of spot activity. For 20 objects photometric periods have been derived, which likely represent the rotation periods. Two objects show persistent variability. For these two, we find a consistent period that is detected in all three datasets. However, this is not necessarily the most significant period in each dataset. This illustrates that periods for individual objects obtained from a single monitoring campaign might not always represent the rotation period. The periods range from 3 to 30 h, with photometric amplitudes from a few mmag to 0.12 mag. We find that we are sensitive to periods longer than 30 h, i.e. the lack of longer periods is not a bias in our dataset. This indicates a lack of slow rotators among VLM objects in this cluster. We confirm that flares are very rare events in very low mass objects.

Compared with solar-mass stars, the very low mass objects in IC4665 show weak photometric variability with low amplitudes, which could be due to a change of spot properties at the fully convective boundary, for example to a

more symmetric spot distribution. Persistent variability is rare, again in contrast to the results for more massive stars. We do not see evidence for differential rotation. One object with persistent periodic variability changes its amplitude by a factor of two over the course of 3 years, while the shape of the lightcurve remains the same, which could be explained by a long-term magnetic cycle. Our sample of lightcurves in IC4665 provides a fundament for future studies of the long-term evolution of activity in the VLM regime.

We find that our periods fit into a scenario where VLM objects experience moderate wind braking in the pre-main sequence phase. They are inconsistent with the strong Skumanich-type wind braking. This is in line with the current paradigm for the angular momentum evolution of low-mass stars, which includes a bimodal nature of the wind braking. We point out that this bimodality is also seen in various properties associated with the magnetic activity, indicating a more fundamental physical difference. While the current parameterised description of wind braking is successful in reproducing main features in the period distributions in open clusters, it does not provide a satisfactory physical picture.

ACKNOWLEDGMENTS

We would like to thank Ansgar Reiners, Sean Matt, Jonathan Irwin, and Jerome Bouvier for instructive discussions regarding topics related to this paper. This work was partially supported by *Deutsche Forschungsgemeinschaft* (DFG) grant Ei 409/11-1 and 11-2.

REFERENCES

- Allain S., Bouvier J., Prosser C., Marschall L. A., Laaksonen B. D., 1996, *A&A*, 305, 498
- Bailer-Jones C. A. L., Mundt R., 2001, *A&A*, 367, 218
- Baraffe I., Chabrier G., Allard F., Hauschildt P. H., 1998, *A&A*, 337, 403
- Barnes J. R., Cameron A. C., Donati J.-F., James D. J., Marsden S. C., Petit P., 2005, *MNRAS*, 357, L1
- Barnes S., Sofia S., 1996, *ApJ*, 462, 746
- Barnes S. A., 2003a, *ApJ*, 586, L145
- , 2003b, *ApJ*, 586, 464
- , 2007, *ApJ*, 669, 1167
- Barnes S. A., Sofia S., Prosser C. F., Stauffer J. R., 1999, *ApJ*, 516, 263
- Berger E., 2006, *ApJ*, 648, 629
- Bouvier J., Forestini M., Allain S., 1997, *A&A*, 326, 1023
- Browning M. K., 2008, *ApJ*, 676, 1262
- Chabrier G., Baraffe I., 1997, *A&A*, 327, 1039
- Chabrier G., Küker M., 2006, *A&A*, 446, 1027
- Cohen R. E., Herbst W., Williams E. C., 2004, *AJ*, 127, 1602
- D’Antona F., Mazzitelli I., 1994, *ApJS*, 90, 467
- Delfosse X., Forveille T., Perrier C., Mayor M., 1998, *A&A*, 331, 581
- Dobler W., Stix M., Brandenburg A., 2006, *ApJ*, 638, 336
- Donati J.-F., Forveille T., Cameron A. C., Barnes J. R., Delfosse X., Jardine M. M., Valenti J. A., 2006, *Science*, 311, 633
- Donati J.-F., Morin J., Petit P., Delfosse X., Forveille T., Aurière M., Cabanac R., Dintrans B., Fares R., Gastine T., Jardine M. M., Lignières F., Paletou F., Velez J. C. R., Théado S., 2008, *MNRAS*, 390, 545
- Durney B. R., De Young D. S., Roxburgh I. W., 1993, *Sol. Phys.*, 145, 207
- Gelino C. R., Marley M. S., Holtzman J. A., Ackerman A. S., Lodders K., 2002, *ApJ*, 577, 433
- Hallinan G., Antonova A., Doyle J. G., Bourke S., Brinken W. F., Golden A., 2006, *ApJ*, 653, 690
- Hawley S., Reid I. N., Gizis J., 2000, in *Astronomical Society of the Pacific Conference Series*, Vol. 212, *From Giant Planets to Cool Stars*, Griffith C. A., Marley M. S., eds., pp. 252–+
- Hawley S. L., Reid I. N., Gizis J. E., Byrne P. B., 1999, in *ASP Conf. Ser. 158: Solar and Stellar Activity: Similarities and Differences*, Butler C. J., Doyle J. G., eds., pp. 63–+
- Helling C., Woitke P., Thi W.-F., 2008, *A&A*, 485, 547
- Herbst W., Dhital S., Francis A., Lin L., Tresser N., Williams E., 2006, *PASP*, 118, 828
- Herbst W., Eisloffel J., Mundt R., Scholz A., 2007, *Protostars and Planets V*, 297
- Herbst W., Mundt R., 2005, *ApJ*, 633, 967
- Horne J. H., Baliunas S. L., 1986, *ApJ*, 302, 757
- Irwin J., Aigrain S., Bouvier J., Hebb L., Hodgkin S., Irwin M., Moraux E., 2009, *MNRAS*, 392, 1456
- Irwin J., Aigrain S., Hodgkin S., Irwin M., Bouvier J., Clarke C., Hebb L., Moraux E., 2006, *MNRAS*, 370, 954
- Irwin J., Hodgkin S., Aigrain S., Bouvier J., Hebb L., Irwin M., Moraux E., 2008a, *MNRAS*, 384, 675
- Irwin J., Hodgkin S., Aigrain S., Bouvier J., Hebb L., Moraux E., 2008b, *MNRAS*, 383, 1588
- Kawaler S. D., 1988, *ApJ*, 333, 236
- Kiraga M., Stepien K., 2007, *Acta Astronomica*, 57, 149
- Lamm M. H., 2003, PhD thesis, PhD Thesis, Combined Faculties for the Natural Sciences and for Mathematics of the Ruperto-Carola University of Heidelberg, Germany (Naturwissenschaftlich-Mathematische Gesamtfakultät der Universität Heidelberg, Germany). XII + 143 pp. (2003)
- Lamm M. H., Mundt R., Bailer-Jones C. A. L., Herbst W., 2005, *A&A*, 430, 1005
- Landolt A. U., 1992, *AJ*, 104, 340
- Matt S., Pudritz R. E., 2008, *ApJ*, 678, 1109
- Meibom S., Mathieu R. D., Stassun K. G., 2009, *ApJ*, 695, 679
- Mermilliod J. C., 1981a, *A&AS*, 44, 467
- , 1981b, *A&A*, 97, 235
- Mestel L., 1984, in *Lecture Notes in Physics*, Berlin Springer Verlag, Vol. 193, *Cool Stars, Stellar Systems, and the Sun*, Baliunas S. L., Hartmann L., eds., pp. 49–+
- Mohanty S., Basri G., 2003, *ApJ*, 583, 451
- Mohanty S., Jayawardhana R., Basri G., 2004, *ApJ*, 609, 885
- Morin J., Donati J.-F., Forveille T., Delfosse X., Dobler W., Petit P., Jardine M. M., Cameron A. C., Albert L., Manset N., Dintrans B., Chabrier G., Valenti J. A., 2008a, *MNRAS*, 384, 77
- Morin J., Donati J.-F., Petit P., Delfosse X., Forveille T., Albert L., Aurière M., Cabanac R., Dintrans B., Fares R., Gastine T., Jardine M. M., Lignières F., Paletou F.,

- Ramirez Velez J. C., Théado S., 2008b, *MNRAS*, 390, 567
Nordhagen S., Herbst W., Rhode K. L., Williams E. C., 2006, *AJ*, 132, 1555
O'dell M. A., Collier Cameron A., 1993, *MNRAS*, 262, 521
Patten B. M., Simon T., 1996, *ApJS*, 106, 489
Pizzolato N., Maggio A., Micela G., Sciortino S., Ventura P., 2003, *A&A*, 397, 147
Prosser C. F., Shetrone M. D., Marilli E., Catalano S., Williams S. D., Backman D. E., Laaksonen B. D., Adige V., Marschall L. A., Stauffer J. R., 1993, *PASP*, 105, 1407
Rebull L. M., 2001, *AJ*, 121, 1676
Reid I. N., Gizis J. E., 1997, *AJ*, 113, 2246
Reiners A., Basri G., 2007, *ApJ*, 656, 1121
—, 2008, *ApJ*, 684, 1390
Roberts D. H., Lehar J., Dreher J. W., 1987, *AJ*, 93, 968
Robin A., Creze M., 1986, *A&A*, 157, 71
Robin A. C., Reylé C., Derrière S., Picaud S., 2003, *A&A*, 409, 523
Rodríguez-Ledesma M. V., Mundt R., Eislöffel J., Herbst W., 2009, in *American Institute of Physics Conference Series*, Vol. 1094, American Institute of Physics Conference Series, Stempels E., ed., pp. 118–123
Saar S. H., 1996, in *IAU Symposium*, Vol. 176, *Stellar Surface Structure*, Strassmeier K. G., Linsky J. L., eds., pp. 237–+
Scargle J. D., 1982, *ApJ*, 263, 835
Scholz A., Coffey J., Brandeker A., Jayawardhana R., 2007, *ApJ*, 662, 1254
Scholz A., Eislöffel J., 2004a, *A&A*, 419, 249
—, 2004b, *A&A*, 421, 259
—, 2005, *A&A*, 429, 1007
—, 2007, *MNRAS*, 381, 1638
Scholz A., Eislöffel J., Froebrich D., 2005, *A&A*, 438, 675
Sills A., Pinsonneault M. H., Terndrup D. M., 2000, *ApJ*, 534, 335
Skumanich A., 1972, *ApJ*, 171, 565
Spiegel E. A., Weiss N. O., 1980, *Nature*, 287, 616
Spruit H. C., van Ballegoijen A. A., 1982, *A&A*, 106, 58
Stassun K. G., Ardila D. R., Barsony M., Basri G., Mathieu R. D., 2004, *AJ*, 127, 3537
Stetson P. B., 1987, *PASP*, 99, 191
Terndrup D. M., Stauffer J. R., Pinsonneault M. H., Sills A., Yuan Y., Jones B. F., Fischer D., Krishnamurthi A., 2000, *AJ*, 119, 1303
Vogt S. S., Hatzes A. P., Misch A. A., Kürster M., 1999, *ApJS*, 121, 547